Journal of Muscle Research and Cell Motility (2006) 27:173–187
DOI 10.1007/s10974-006-9056-7

The stroke size of myosins: a reevaluation

BERNHARD BRENNER*
Department of Molecular and Cell Physiology, Medical School Hannover, Carl-Neuberg-Street 1, D-30625, Hannover, Germany

Received 16 December 2005; accepted in revised form 9 January 2006

Abstract

In this article results are reviewed from different experimental approaches to determine the size of the power stroke generated by myosin molecules during their ATPase cycle. While data from fiber studies and protein crystallography predict a stroke size of about 10 nm for skeletal muscle myosins, single molecule studies imply a stroke size for these myosins of only about 5 nm. Single molecule studies also showed the stroke size to be proportional to the length of the light chain binding domain, acting like a lever arm. At the same lever arm length, however, the stroke size of smooth muscle myosin II is found about twice as large and a stroke size of about 14 nm was reported for class-I myosins. It was proposed that such different stroke sizes for molecules with same lever arm length result from different extend of converter domain rotation. Only for class-I myosins, however, an about 30° larger rotation of the converter was found so far by protein crystallography. This, however, is far too small to account for the almost 3-fold larger stroke size reported from single molecule studies. In this contribution we discuss some factors that might account for the apparent discrepancies between single molecule studies on the one hand and protein crystallography as well as some fiber studies on the other hand. In addition, we present some modeling to illustrate that the power stroke very likely is underestimated to a large extent in current single molecule approaches. We further show that differences in the stroke size for various classes of myosins reported from single molecule studies might be related to small differences in the probability to execute the power stroke kinetics. We demonstrate that such small changes in power stroke kinetics can seriously affect the extent to which the 'true' power stroke is underestimated by present single molecule approaches.

Introduction

Motor proteins of the myosin family drive motile events by a multi-step power stroke. This multi-step power stroke is composed of a series of structural changes within the actin–myosin complex after the myosin motor domain has attached to an actin filament. Each of these structural changes is thought to be associated with a specific reaction step in the acto-myosin-ATPase cycle. Without external load the total movement generated by one head of a myosin molecule during an ATPase cycle is expected to be equal to the sum of the individual structural changes that are part of the multi-step power stroke.

Due to the fundamental relevance of the power stroke for driving motile events, the structural basis of the power stroke, its connection to mechanical forces and movements, as well as its link to the intermediates of the ATPase cycle are central to the understanding of how hydrolysis of ATP drives motile events. Due to the close link between structural, mechanical and biochemical events, a large variety of experimental approaches have been used to elucidate the molecular processes underlying the power stroke. As a consequence, different experimental approaches have yielded information about the processes associated with the power stroke and about the distance over which a myosin head can drive the sliding of an actin filament during its power stroke. Although there is, with few exceptions, agreement about the order of magnitude over which a myosin head can drive filament sliding, closer comparison between estimates from muscle fiber studies, protein crystallography, and single molecule experiments appeared to reveal some systematic discrepancies.

In this contribution we first summarize the main conclusions about the stroke size drawn from fiber studies. We then summarize the main findings from single molecule experiments, including effects of different lever arm lengths on the observed stroke size. We compare these results with some structural data to highlight some of the discrepancies. Finally, we present some modeling work that was initiated by a recent contribution by Sleep and coworkers (Sleep *et al.*, 2005). This modeling allowed to identify possible sources for the observed discrepancies. We will illustrate some factors that very likely have resulted in an underestimate of the size of the power stroke in

* To whom correspondence should be addressed. Phone: +49-511-532-6396; Fax: +49-511-532-4296; E-mail: Brenner.Bernhard@MH-Hannover.de

previous single molecule experiments, including our own.

Displacement generated during the power stroke: results of fiber experiments

Several early attempts to determine the size of the power stroke of skeletal muscle myosins were based on trials to measure ATP hydrolysis in muscle fibers or myofibrils during lightly loaded or unloaded shortening (Homsher *et al*., 1981, Yanagida *et al*., 1985, Brenner, 1988, Harada *et al*., 1990, Higuchi and Goldman, 1991). Together with estimates of the duty ratio, i.e., the time of an ATPase cycle over which a myosin head stays strongly attached to an actin filament such ATPase measurements were used to estimate the distance of actin filament movement over which a myosin head stays strongly attached to an actin filament during high speed shortening. This distance was found in the order of ≥40–50 nm (summarized by Burton (1992)).

In muscle fibers, however, many myosin molecules act in parallel. As a consequence, the movement of an actin filament relative to a myosin filament results from the action of many myosin heads. Thus, the total movement of an actin filament while an individual myosin head is strongly bound to the actin filament is not only the result of the structural changes during the multi-step power stroke of this myosin head. Instead, if the strongly bound myosin head does not dissociate in time it will be pulled along due to the action of other myosin heads that continue to move the actin filament. Thus, a myosin head that stays attached after completion of its 'active' power stroke will be pulled beyond the reach of its 'active' stroke. Beyond its active stroke this myosin head will start to generate increasing forces that oppose further movement of the actin filament (cf. Huxley, 1957). In fact, the maximum speed of filament sliding in a muscle fiber was proposed to adjust itself such that at the maximum speed of filament sliding active driving forces from myosin heads undergoing their 'active' power stroke will be balanced by forces opposing movement by myosin heads that have ended their power stroke but have not yet dissociated from the actin filament (Huxley, 1957). With this concept the total movement of an actin filament while a myosin head stays strongly attached equals the sum of the 'active stroke' plus the 'drag stroke' (cf. Pate *et al*., 1993). Thus, the above-mentioned estimate of ≥40–50 nm is expected to be much larger than the 'active' multi-step power stroke. Based on mechanical and kinetic data obtained from different myosin isoforms and with different substrates, Pate and coworkers tried to separate the 'active' stroke from the 'drag' stroke. With this approach they estimated an active stroke of approximately 10 nm (Pate *et al*., 1993). In more recent trials, Lombardi and coworkers (Piazzesi *et al*., 2002; Reconditi *et al*., 2004) tried to separate the 'active' power stroke within the transient response at the beginning of muscle shortening after sudden unloading. With decreasing load during fiber shortening, the observed power stroke approached about 7 nm. From modeling work it was estimated that without truncation by early detachment of some myosin heads the active power stroke should be in the order of about 10 nm (Piazzesi *et al*., 2002).

In a different type of experiment the ability of muscle fibers to recover active force after sudden length releases was studied (quick release experiments; e.g., Huxley and Simmons, 1971, 1973; Ford *et al*., 1977). In these experiments the distance over which a cross-bridge can generate active force and movement initially appeared to be in the order of 15–20 nm (Huxley and Simmons, 1971). In later, faster measurements this distance was found to be about 14 nm (Ford *et al*., 1977). Assuming no compliance in actin and myosin filaments, this result was thought to be consistent with an overall power stroke of about 14 nm. X-ray diffraction studies, however, revealed significant compliance in actin and myosin filaments (Huxley *et al*., 1994, Wakabayashi *et al*., 1994). Thus, the 'active' power stroke very likely is substantially shorter than the about 14 nm of filament sliding over which force recovery can be observed after a rapid length.

In summary, muscle fiber studies altogether appear consistent with a power stroke in the order of about 10 nm, i.e., a distance of 10 nm over which myosin heads can (actively) drive filament sliding.

Displacement generated during the power stroke: results from single molecule studies

A first attempt to detect forces and movements when individual myosin molecules or fragments of myosin molecules interact with an actin filament was introduced by Finer *et al*. (1994). In this approach, two microspheres are attached to an actin filament, e.g., by NEM-modified myosin. Each bead is held by an independently adjustable trap such that the actin filament can be pre-tensioned beyond slack length. This 'dumbell'-arrangement is steered on top of a third, larger bead which is immobilized on a cover slip and coated with nitrocellulose. After sparsely coating of the nitrocellulose layer with myosin, S1, HMM, or constructs of myosin molecules, individual interactions of the molecules with the suspended actin filament can be detected (Figure 1).

On the basis of this 'three-bead assay', Molloy *et al*. (1995) developed an approach to determine the stroke size generated by single S1-, or HMM-molecules. Molloy and coworkers found that upon binding of the suspended actin filament to a myosin molecule the thermal fluctuations of the dumbell are reduced, as expected by an increase in overall stiffness when the dumbell is tethered to the third bead by the S1- or HMM-molecule. Using this reduction in thermal fluctuations as the signature to identify binding events,

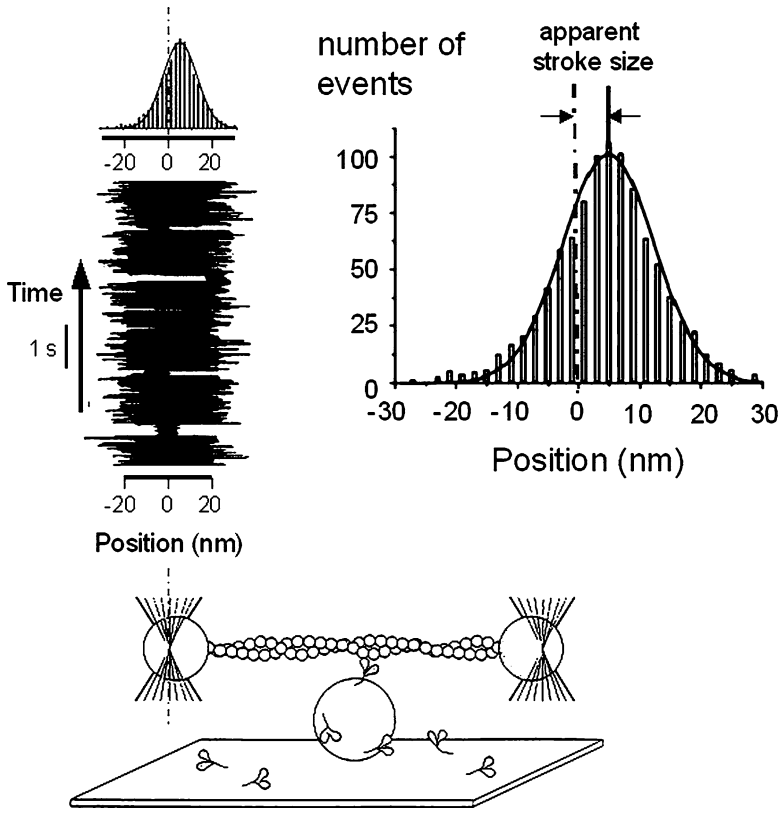

Fig. 1. Scheme of the three-bead experimental arrangement. Bead at left end of suspended actin filament is imaged onto a quadrant detector. Noise on position signal represents thermal fluctuations of actin filament with attached beads (dumbell) while freely suspended in the two traps. Transient reductions in amplitude of thermal fluctuations were interpreted as events of binding of myosin head to actin filament resulting in increased overall stiffness (Molloy *et al.*, 1995). Histograms of mean bead position during binding events are found to be offset from mean position observed while dumbell is free (no myosin head attached). According to Molloy and coworkers (1995), the shift of the histogram relative to mean position of free dumbell (labeled 'apparent stroke size') is interpreted to represent displacement generated by individual HMM or S1 molecules during their interaction with the actin filament (modified from Molloy *et al.*, 1995; Finer *et al.*, 1994).

Molloy and coworkers generated a histogram of the actual bead positions observed during the various binding events. Histograms generated from a large number of binding events were found to be well described by a Boltzmann distribution. The width of this distribution is essentially identical with the width of thermal fluctuations of the free dumbell and is determined by the overall stiffness of the two traps by which the dumbell is suspended. The histogram of actual dumbell positions during the binding events, however is not centered around the equilibrium position of the free dumbell but was found to be shifted to one side relative to the time averaged position of the free dumbell (zero-position in Figure 1, indicated by vertical dashed-dotted line). The direction of this shift was found to be determined by the polarity of the suspended actin filament (Molloy *et al.*, 1995).

The shift of the position histogram was interpreted to represent the filament sliding generated during the power stroke of the S1 and HMM molecules on the third bead. Thus, the amplitude of the shift of the histogram against the mean position of the free trap was considered to represent the amplitude of the power stroke, i.e., the amplitude of the structural changes associated with the power stroke.

For this interpretation Molloy and coworkers assumed that cross-bridge attachment occurs with equal intrinsic probability over the full range of the Brownian motion of the actin filament. As one basis for this assumption, actin filaments (and trapped beads) were thought to freely rotate in an unconstrained fashion such that on average every actin monomer is equivalent, i.e., actin monomers do not form target zones (Molloy *et al.*, 1995). A further, more hidden assumption was that after initial attachment the probability to execute the power stroke will also occur with equal intrinsic probability over the full range of the Brownian motion of the actin filament.

In later experiments with a feedback stabilized system and with only a single myosin molecule probed over time, the helical arrangement of the actin monomers within the filament was found to modulate the probability of binding along an actin filaments, equivalent to the organization of binding sites on the actin filament in so called 'target zones' (Steffen *et al.*, 2001). In less stable equipment or when individual events of several different myosin molecules are accumulated, such target zones, however, are averaged out and not detectable. Instead, the probability distribution of individual events essentially follows the probability distribution of

the dumbell position during thermal fluctuation (Molloy *et al*., 1995; Tanaka *et al*., 1998; Ruff *et al*., 2001b; Kohler *et al*., 2003).

With some class I myosins, e.g., myosin IB or myosin IA, it was found that displacement can take place in two distinct steps (Veigel *et al*., 1999). For analysis of the amplitude and timing of the second step, individual binding events were aligned according to their beginning, and, in a second plot, according to their ending (Veigel *et al*., 1999). When the aligned individual events were added up the average displacement at the beginning and the end of the binding events can be compared. A larger displacement from the equilibrium trap position at the end of a binding event is interpreted as evidence for a second structural change contributing to the overall power stroke. The time course of the averaged individual events allows to determine (i) the probability (rate constant) for the second structural change to occur or (ii) the probability of an ATP-binding to the empty nucleotide binding site that ends the interaction event (Veigel *et al*., 1999). In this analysis, however, again the two basic assumption are made that (i) initial binding occurs with equal probability throughout the range of thermal fluctuations of the actin filament, and that (ii) the power stroke can be executed with equal probability throughout the full range of Brownian motion of the dumbell.

The apparent stroke size is proportional to the length of the light chain binding domain. On the basis of the concept of Molloy and coworkers to determine the size of the power stroke we attempted to directly test the hypothesis that the light chain binding domain functions as a lever arm. This hypothesis was initially proposed on the basis of the crystal structure of S1 (Rayment *et al*., 1993a, b) and had been tested by studies of the actin gliding velocity driven by myosin constructs with (i) different number of light chain binding sites (Uyeda *et al*., 1996) and with (ii) artificial lever arms of different lengths (Anson *et al*., 1996). We directly tested the prediction of the lever arm hypothesis, i.e., that the stroke size of myosin II constructs should be proportional to the length of the lever arm, by recording the apparent stroke size of the constructs with different artificial lever arm lengths (Anson *et al*., 1996). We determined the apparent stroke size according to the approach introduced by Molloy and coworkers (1995). The results showed a linear relation between the lever arm length determined from the known structure of the artificial lever arms and the apparent stroke size determined by a needle trap system (Figure 2, data labeled DdII; Ruff *et al*., 2001b). Our assay system was essentially identical with the three bead arrangement (cf. Figrue 1; Finer *et al*., 1994; Molloy *et al*., 1995) except that one of the two beads by which the actin filament is suspended was replaced by a microneedle. All myosin II constructs were found to generate an apparent stroke size that falls within or near the 95% confidence range of a linear relation (Figure 2). Furthermore the linear relation does not extrapolate to a lever arm

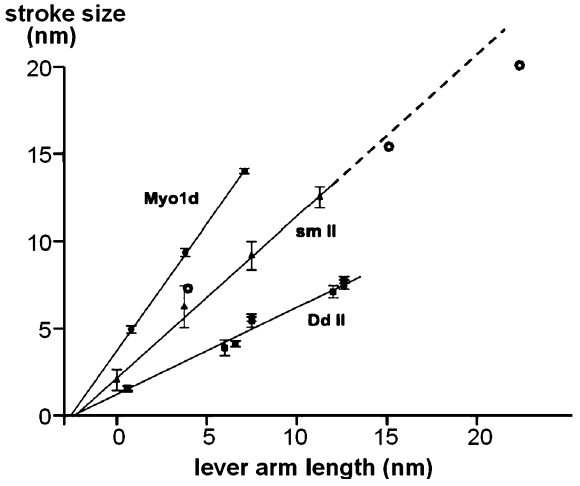

Fig. 2. Plots of observed stroke size vs. lever arm length for *Dictyostelium discoideum* myosin II (DdII; Ruff *et al*., 2001b), smooth muscle myosin II (smII; Warshaw *et al*., 2000) and rat myosin 1d (Myo 1d). Open circles are data of myosin V constructs with 1, 4, and 6 IQ-motives (Purcell *et al*., 2002). Solid lines are best fits of linear regression analysis, the dashed line is an extension of the fit to the smooth muscle myosin II data points (modified from Kohler *et al*., 2003).

length of 0 nm but rather to a lever arm length of about −2 nm. This was interpreted to be consistent with the concept that the hinge point of the lever arm is located about 2 nm inside the catalytic domain near Gly 691 at the distal end of the SH1 helix. From structural studies, this Gly 691 was thought to represent the hinge point of converter domain movement (Geeves and Holmes, 1999). The apparent stroke size observed for HMM and S1 constructs with native essential and regulatory light chains was 5.5 and 5.4 nm, respectively (Ruff *et al*., 2001b).

From the observed stroke size, the known structure of the constructs (Kliche *et al*., 2001), and with the assumption that the plane of lever arm rotation is aligned with the actin filament axis, the lever arm rotation during the power stroke was expected to be about 30° (Ruff *et al*., 2001b). This appeared in reasonable agreement with the about 20° rotation estimated from fluorescence polarization studies with fluorescent probes attached to the light chain binding domain in fibers (Corrie *et al*., 1999). The estimated 30° of lever arm rotation, however, are about half the rotation expected from protein crystallography (see below).

For the same lever arm length the size of the apparent power stroke can vary among different myosins. A similar linear relation of apparent stroke size vs. lever arm length was also reported for smooth muscle myosin II (Warshaw *et al*., 2000; cf. smII in Figure 2), and for single headed myosin V constructs (Purcell *et al*., 2002; cf open circles in Figure 2). The lever arm length for the two myosins were varied by the number of IQ domains in the constructs. Comparison of stroke sizes reported for chicken myosin II (Molloy *et al*., 1995), chicken myosin 1a and rat myosin 1b (Veigel *et al*., 1999), chicken smooth muscle myosin II (Warshaw

et al., 2000), *Dictyostelium discoideum* myosin II (Ruff *et al*., 2001b), as well as myosin V (Purcell *et al*., 2002; Tanaka *et al*., 2002), suggested that the observed stroke sizes are not directly related to the assumed lever arm lengths. Therefore, in one study with the same equipment and the same experimental conditions the data obtained from *Dictyostelium discoideum* myosin II were extended by stroke size measurements on rat myosin1d with different number of light chain binding sites (Myo 1d in Figure 2; Kohler *et al*., 2003). For each of the sets of myosin constructs the observed stroke size showed a linear dependence on the lever arm length, but the slopes of the relations were quite different. This was interpreted to indicate that different motor domains can generate different degrees of converter domain rotation and thus different degree of lever arm movement while the axis of rotation is located at a similar position inside the motor domain (Kohler *et al*., 2003).

The data for single headed myosin V constructs with different lever arm lengths again showed a nearly linear dependence between stroke size and lever arm length. These data, however, may extrapolate to an axis of rotation that is much further inside the catalytic domain (cf. Figure 3b of Purcell *et al*., 2002). If the stroke sizes of single headed myosin V constructs, however, are compared with the other data in Figure 2, especially the data for myosin V constructs with one and four IQ domains tend to fall near the range of the smooth muscle myosin II constructs. The increasing deviation toward smaller apparent stroke sizes at longer lever arm lengths may be due to limited rigidity of the long light chain binding domain with 6IQ domains.

In summary, the observed stroke size for a lever arm length of two IQ-domains is about 5.5 nm for *Dictyostelium discoideum* myosin II. The observed stroke size for smooth muscle myosin II and single headed constructs of chicken myosin V is about 9 nm and thus more than 60% larger than for the *D. discoideum* myosin II. For rat myosin 1d with two IQ domains the observed stroke size is about 14 nm, i.e., almost three-times the stroke size of *D. discoideum* myosin II. The differences were discussed in terms of different amplitude of lever arm movement of the various myosins (Kohler *et al*., 2003).

Displacement generated during the power stroke: magnitude expected from structural studies

In myosin II of chicken or Dictyostelium discoideum *converter domain is rotated about* 70°. Assuming that in the pre-power stroke state the catalytic domain docks onto the actin filament with the same orientation as in the post-power stroke state, i.e., assuming that no redocking contributes to the re-orientation of the lever arm during the cross-bridge cycle, a 70° rotation of the lever arm is expected, starting and ending at the two orientations shown in Figure 3a. Such 70° rotation of the converter/light chain binding domain could drive filament sliding over a distance comparable to the length of the effective lever arm. This is the distance between the axis of rotation and the hinge at the tip of the lever arm which connects the lever arm to the rod part of the myosin molecule.

For such a geometry we should expect a filament sliding of about 10 nm for a myosin II molecule with a native lever arm of $7.5+2=9.5$ nm. The 7.5 nm equal the length of the light chain binding domain with two IQ-motives. The 2 nm are the distance between the basis of the light chain binding domain and the hinge point of lever arm rotation which from structural studies cf. (Geeves and Holmes, 1999) seems to be about 2 nm inside the catalytic domain. Note that the stroke size of about 9.5–10 nm expected from structural studies for myosin II of skeletal muscle is essentially identical with the size of the active power stroke derived by several approaches from muscle fibers.

Rotation of the light chain binding domain of class I myosins is about 30° *larger than for myosin II*. The crystal structure of a class-I myosin construct (Kollmar *et al*., 2002) with $MgADP.VO_4$ in the active site shows a somewhat more pronounced kink in the relay helix. This positions the converter in the 'pre-power stroke' state about 30° further 'up' than in myosin II structures (Kollmar *et al*., 2002). As a consequence, it was proposed that class I myosins can produce a power stroke about 20–30° larger than the 60–70° rotation of the myosin-II lever arm. Image reconstructions of actin filaments decorated with class-I myosins showed that in the rigor state the orientation of the catalytic domain on the actin filament is virtually indistinguishable from class-II myosins (Jontes *et al*., 1995, 1998; Jontes and Milligan, 1997, Carragher *et al*., 1998). It was therefore assumed that the nucleotide-free rigor complex has similar geometry as seen for reconstructions with class-II myosins (Schroder *et al*., 1993). On this basis, the three orientations for the light chain binding domain for class-II and class-I myosins was constructed (Figure 3b; Kollmar *et al*., 2002). These structures predict about 30–35% larger axial movement of actin filaments relative to the myosin filaments for class-I myosins compared to the movement generated by class-II myosins with same lever arm length. Note that this is much smaller than the increase in stroke size seen in single molecule experiments. The stroke size of class I myosin was reported to be about 2.5- to 3-times the stroke size of skeletal muscle myosin II (Kohler *et al*., 2003).

In summary, from protein cystallography of *Dictyostelium discoideum* myosin II constructs an about two-times larger stroke sizes is expected than the stroke size seen in single molecule experiments with the histogram technique. The increase in stroke size from *Dictyostelium discoideum* class-II myosins to class-I myosins expected from structural studies, in contrast, is much smaller than the increase in stroke size reported from

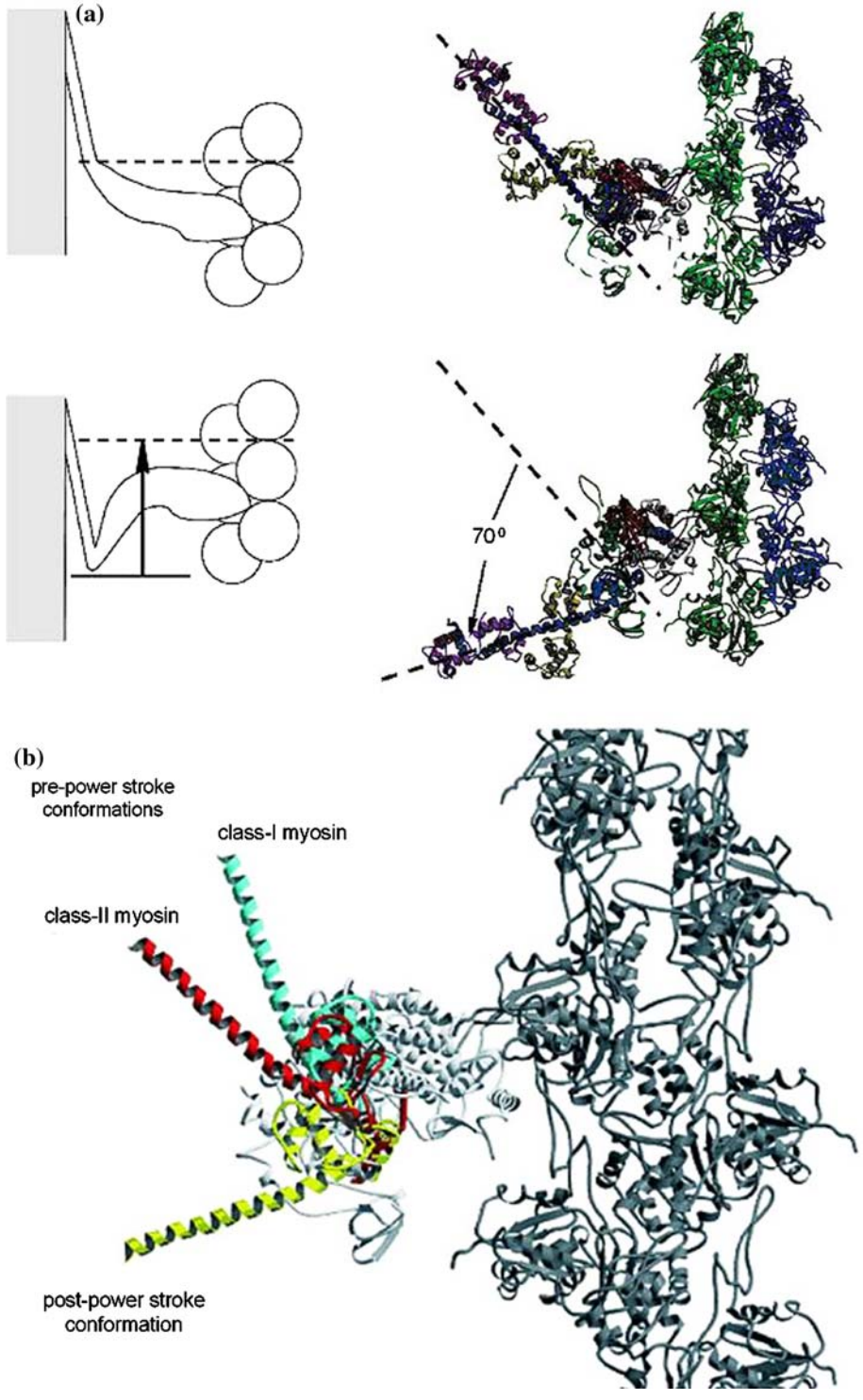

Fig. 3. (a) Structural changes driving filament sliding in the rotating lever arm concept. Left panel, illustration of the arrangement of the myosin head with catalytic domain and light chain binding domain relative to actin and myosin filaments (modified from Cooke, 1986). Rotation of the light chain binding domain while the catalytic domain is fixed at the actin filament results in a sliding of the actin filament relative to the myosin filament back bone. Distance and direction of actin filament movement is indicated by arrow. Distance of movement equals movement of end of light chain binding domain relative to catalytic domain. Right panel shows "pre-power stroke" (top) and a "post-power stroke" crystal structures of myosin head domain fit to atomic model of actin filament. "Post power stroke structure" is chicken S1 (Rayment *et al*., 1993a) docked onto actin filament structure (Schroder *et al*., 1993; Geeves and Holmes, 1999). "Pre-power stroke" structure is ADP.vanadate-structure (Smith and Rayment, 1996) with light chain binding domain of chicken S1 (Rayment *et al*., 1993a) modeled on structure of truncated myosin head domain of *Dictyostelium discoideum* myosin II. Model of pre-power stroke structure is docked onto actin filament assuming same orientation of catalytic domain relative to actin filament as for post power stroke geometry (Geeves and Holmes, 1999). Note that in pre-power stroke orientation lever arm is rotated 70° relative to the post-power stroke structure (modified from Geeves and Holmes, 1999). (b) Docking of class-I and class-II myosin crystal structures onto actin filament model. α-helix of light chain binding domain (Rayment *et al*., 1993) modeled onto crystal structures of truncated class-I myosin head domains to illustrate orientation of lever arm expected from position of converter domain (modified from Kollmar *et al*., 2002).

single molecule studies. Thus, the degree of discrepancy between stroke sizes expected from structural studies vs. stroke sizes derived in single molecule experiments with the histogram technique varies for different members of the myosin superfamily.

Factors that may contribute to discrepancy between expected stroke size and stroke size observed in single molecule measurements

Arrangement of binding sites on actin filaments in target areas. One possible source of uncertainties in stroke size estimates with the histogram approach (Molloy *et al*., 1995) or related event averaging techniques (Veigel *et al*., 1999) is the organization of binding sites on actin filaments in form of target areas. This limits the assumption of equal probability of attachment to any point along an actin filament (Steffen *et al*., 2001). However, systematic scanning, or sampling of individual interaction events from more than one myosin molecule on the third bead, as well as drift in the system during long periods of data collection average out effects arising from organization of binding sites in target areas (Steffen *et al*., 2001). The published histograms on which the apparent stroke size data are based (Tanaka *et al*., 1998; Ruff *et al*., 2001b; Kohler *et al*., 2003) do not show the characteristic signs described for interactions that are restricted to target areas (Steffen *et al*., 2001). Thus, restriction of interactions to target areas appears unlikely to account for discrepancies between fiber data and structural studies on the one hand and the apparent stroke size derived from single molecule experiments on the other hand.

Random orientation of myosin heads relative to actin filament axis. A second source proposed to cause reduction in observed stroke sizes is the random orientation of S1 and HMM molecules on the third bead (Tanaka *et al*., 1998). This proposal was based on displacement histograms constructed from individual interactions between actin filaments and filaments formed from single headed myosin molecules and myosin rod fragments. Deviation from parallel alignment of actin filament and myosin/myosin rod co-filament appeared to reduce the observed shift in the position histogram (Tanaka *et al*., 1998). Assuming a stroke size of 0 nm when the axis of the suspended actin filament is perpendicular to the myosin/myosin rod co-filament axis, Tanaka *et al*. (1998) estimated that the observed average stroke size for randomly oriented myosin heads should be about 50% of the stroke size seen for parallel orientation of actin filament and myosin/myosin rod co-filament. In an essentially identical experimental approach, however, no orientation dependence of the apparent stroke size could be detected (Ruff *et al*., 2001a).

Trapping forces may affect probability to initiate power stroke after initial attachment. Not only the histogram technique of Molloy and coworkers, but also the event averaging technique of Veigel *et al*. (1999), and the variance analysis (Guilford *et al*., 1997) are all based on two main assumptions. (i) Binding of myosin heads to actin is assumed to occur with identical probability at any position along the actin filament (cf. Molloy *et al*., 1995), and (ii) the power stroke after initial attachment is assumed to occur with equal probability at all positions along the actin filament. This second point was recently questioned by Sleep and coworkers (Sleep *et al*., 2005). It was pointed out that forces generated by the two traps will introduce distortion of the attached myosin head resulting in non-equal probability to execute the power stroke which eventually might lead to reduction in the observed stroke size. Previously, effects from distortion of the myosin head by trapping forces were considered irrelevant at the usual trap stiffnesses since distortions of the myosin head domain are very small as long as trap stiffness is much smaller than the stiffness of the attached myosin head.

Distortion of attached myosin heads by trapping forces

Qualitative estimate of effects on apparent power stroke determined by histogram technique

Figure 4 illustrates the three bead arrangement and the effects expected from distortion of tethered myosin head domains by trapping forces acting on the two beads by which the actin filament is suspended. Consider attachment of a myosin head to the actin filament while the beads of the dumbell, due to their thermal fluctuations, are outside the center of their traps (cf. event 1 in Figure 4). In this case the attached myosin head will be distorted by the trapping forces that tend to drive the two beads toward their equilibrium position at the centers of their traps. Since trap stiffness is much lower than stiffness of the attached myosin head, the distortions of the attached myosin head will be small. Nevertheless, it is expected that such distortions will result in some non-equal probability of the myosin head to proceed from the initially attached state (state 1 in Figure 4) to state 2. The probability to proceed into the power stroke is expected to be increased if attachment takes place while the dumbell is to the left of the trap center (cf. event 2 in Figure 4) and will be decreased if the dumbell is to the right of the trap center when the myosin head attaches to the actin filament (event 1).

As a consequence, the observed shift of the position histogram will be different from the displacement generated during the power stroke. This is illustrated in Figure 5. If at all positions of the dumbell the initially attached myosin head will proceed into the power stroke with the same probability, then the shift of the position histogram equals the filament sliding generated by the power stroke (green curve vs. red curve in Figure 5b; Molloy *et al*., 1995). With non-equal

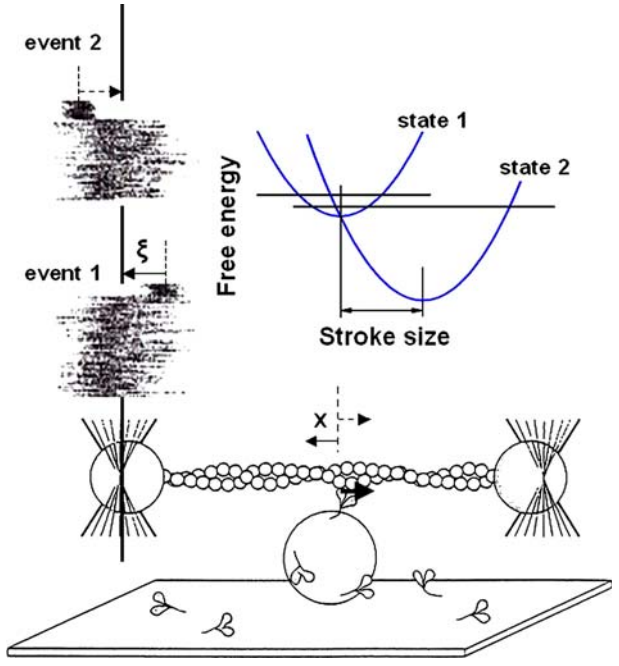

Fig. 4. Scheme of distortions of myosin head generated in the dumbell system. Event 1: attachment of myosin head to actin filament while, by thermal agitation, dumbell is positioned near to extreme right of thermal fluctuations. At this position trap pulls dumbell back toward center of trap (solid horizontal arrow toward vertical solid line; vertical solid line represents equilibrium position of trap). Trapping forces that pull dumbell back toward trap center along actin filament axis generate distortion of tethered myosin head (solid arrow away from vertical dashed line. Dashed line represents undistorted position of tethered myosin head). Distortion of tethered myosin head is against direction of movement generated during the power stroke (heavy solid arrow pointing to right from undistorted position of tethered myosin molecule). When elastic forces are balanced the ratio of head distortion (x)/dumbell displacement from trap center (ξ) is proportional to ratio of head stiffness (k_{head})/combined trap stiffness (k_{trap}). Distortion of myosin head is opposite to direction of power stroke and thus reduces probability to proceed into the power stroke, i.e., to proceed from the initially attached state (state 1) to state 2. Event 2: Attachment of myosin head takes place while thermal fluctuations have driven dumbell to far left of range of thermal fluctuations. Thus, while myosin molecule is bound to actin filament and keeps dumbell near the far left of thermal fluctuations, dumbell experiences trapping force that pulls toward center of trap (dashed arrow toward vertical solid line = center of trap along actin filament axis). Thus, attached myosin head is pushed in shortening direction (dashed arrow pointing away from dashed vertical line). This favors transition into power stroke, i.e., from initially attached state 1 to state 2. ξ, displacement of dumbell from equilibrium position; x, distortion of myosin head. Direction of power stroke indicated by heavy solid arrow pointing to right from attached myosin head.

probability to proceed into the power stroke, e.g., as illustrated in Figure 4, however, the frequency of events will increase on the left part of the shifted position distribution (upward arrows on green curve in Figure 5c) and decrease on its right side (down arrows in Figure 5c). Overall, this will result in a reduced shift of the actually observed position histogram (black curve in Figure 5d). Thus, qualitatively the observed shift in the position histogram and thus the 'observed' stroke size is expected to be smaller than the actual filament sliding generated when the initially attached myosin head proceeds into the power stroke (to state 2 in Figure 4).

Quantitative modeling of expected effects on stroke size determined by histogram technique

To evaluate the relevance of possible effects of trapping forces on the observed stroke size in the histogram analysis and the related event averaging technique we examined possible effects of trapping forces by using a model for cross-bridge action that we had previously proposed (Brenner, 1990; Chen and Brenner, 1993). After initial, rapid-equilibrium attachment, the power stroke is assumed to take place in a reversible reaction step, e.g. from an AM.ADP.Pi-state to an AM.ADP state. For the results presented in the subsequent section, the exact assignment of the biochemical intermediates, however, is not essential. The assumptions made for the modeling are specified in each part as they are introduced. The free energy functions are included schematically in Figure 4 to illustrate their relation to the experimental arrangement. In Figure 6, the relevant free energy functions are shown together with a possible set of rate functions used in the modeling. Note that different from earlier convention (cf. Huxley, 1957; Hill, 1974) direction of active movement is to the right. This is to account for the direction of the shift in the histograms generated in the analysis of single molecule experiments (Molloy *et al.*, 1995). Usually this shift, attributed to the power stroke, is shown as movement to the right. To minimize complexity, at this stage we assume two actin attached states, an initially attached state with no average displacement (state 1) and a second state (state 2) for which displacement along the actin filament of 10 nm is assumed (for convenience). For both states the corresponding detached state is also specified (labeled '1' and '2'). Only for the second state the free energy minimum is assumed far below the related detached state; i.e., the first state has much lower actin affinity than the second. For quantitative modeling a linear elasticity was assumed for the attached myosin head, and for both states the stiffness was assumed to be 1 pN/nm. Accordingly, the two free energy functions are parabolas of same shape. The horizontal shift of their minima is the amplitude of the stroke associated with the reaction step from the initially attached (state 1) to the second, strongly attached state (state 2). For convenience, this displacement was assumed to be 10 nm. The vertical shift between the free energy functions of state 1 and state 2 was adjusted such that the free energy function of the second attached state (state 2) crosses the free energy profile of the first attached state (state 1) at its minimum (cf. Figure 6). This is a frequently used, but non-crucial assumption in previous modeling (cf. Hill, 1974).

With the assignments for stiffness of the myosin head and thus for the shape of the free energy functions of the attached states (state 1 and state 2), as well as for

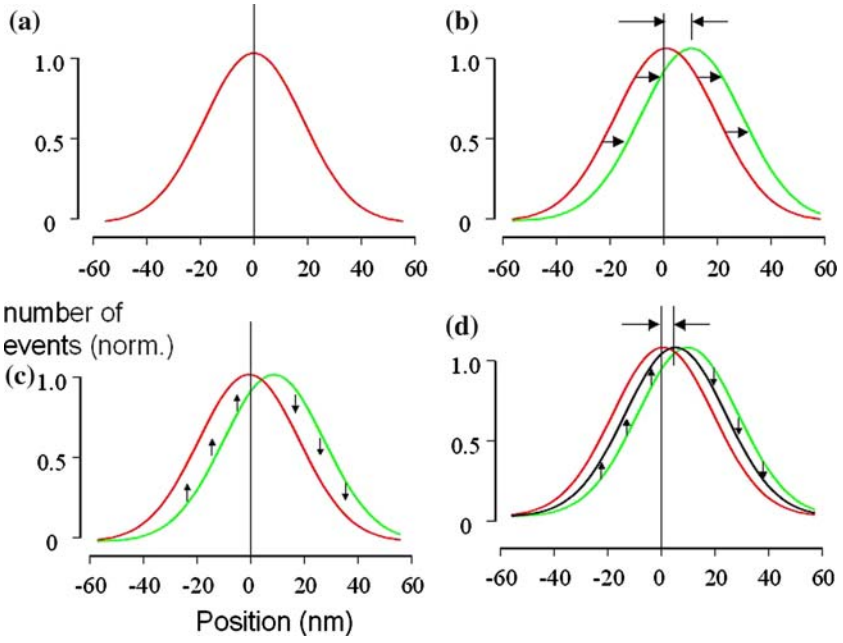

Fig. 5. Apparent stroke size for a system with distortion of attached myosin heads by trapping forces. Schematic illustration of effects on histogram analysis. (a) Position histogram of free dumbell (= red Gaussian function in all graphs). (b) Histogram of dumbell position during binding events (green Gaussian function). Assumption: strain-independent probability to initiate the power stroke after initial attachment; assumed power stroke = 10 nm. Horizontal arrows indicate shift of histogram of trap position during binding events. Such shift is expected to reflect filament sliding initiated by power stroke; e.g., 10 nm in this example. (c) Downward arrows illustrate effects from reduced probability to execute power stroke (trapping forces generate strain against direction of power stroke) vs. upward arrows illustrating increased probability of power stroke (trapping forces generate strain in direction of power stroke). (d) Black Gaussian function represents position histogram during binding events expected from (c). Note that observed shift of histogram (black trace vs. red trace) is much less than 10 nm.

the relative position of the free energy functions, the free energy changes (ΔG) associated with initial attachment and with the transition from the initially attached state 1 to state 2 ($\Delta G_{1,2}$) is determined for any distortion (x) of the myosin head ($\Delta G_{1,2}(x)$). From the difference in free energy associated with the various reaction steps the equilibrium constants (e.g., $K_{1,2}(x)$) of these reactions are also determined for any distortion of the myosin head. For instance,

$$K_{1,2}(x) = \exp(-\Delta G_{1,2}(x)/k_B T)$$

where $\Delta G_{1,2}(x)$ is the free energy difference between the two attached states at different distortion x; k_B is Boltzmann constant, and T is the absolute temperature.

From the equilibrium constants at a given distortion, however only the ratio of the forward over the reverse rate constant is known.

In our modeling eventually different assumptions were made for the x-dependence of the two rate constants. Initially, the frequently used assumption of equal partitioning of strain dependence between forward and reverse rate constant was made. The corresponding rate functions for the transition from state 1 to state 2 are also shown in Figure 6. We did, however, not limit our modeling to this assumption.

We further assumed that myosin heads can attach at any position along the actin filament; i.e., the probability to attach to actin at a specific position of the dumbell (ξ) is determined by the thermal fluctuation of the dumbell in the two traps. Thermal fluctuation of the dumbell results in a Gaussian-shaped histogram for initial attachment, located at the center of the trap (cf. Figure 5a). For the distortion (x) of the attached myosin head by the trapping forces acting on the two beads of the dumbell, it was assumed that the trapping forces and forces of elastic distortion of the attached myosin head are of equal magnitude but opposite direction. Thus, the ratio of dumbell displacement (ξ) from its free average position over the elastic distortion of the attached myosin head (x) equals the ratio of head stiffness (k_{head}; 1 pN/nm) over the stiffness of the two traps (k_{trap}; e.g., 0.01 pN/nm). Consequently, head distortion (x) during an event was usually only in the order of 1/100 of the dumbell displacement (ξ) from its mean free position.

To mimic the actual experimental situation we also assumed (at this stage) that essentially each event that has proceeded into the second, strongly attached state will be detected by reduced thermal fluctuation while the initial (weak) attachment is too short to be detectable with currently available time resolution of the measurements.

In the first step of the modeling, the distribution of dumbell positions, $P(\xi)$, during free thermal fluctuation was calculated ($P(\xi) = \exp(-1/2 k_{trap}\xi^2/k_B T)$). In the second step, the head distortion (x) in the initially attached state was determined. Head distortion was obtained from balance between trapping forces ($F_{trap}(\xi) = k_{trap}\xi$) and elastic forces resulting from

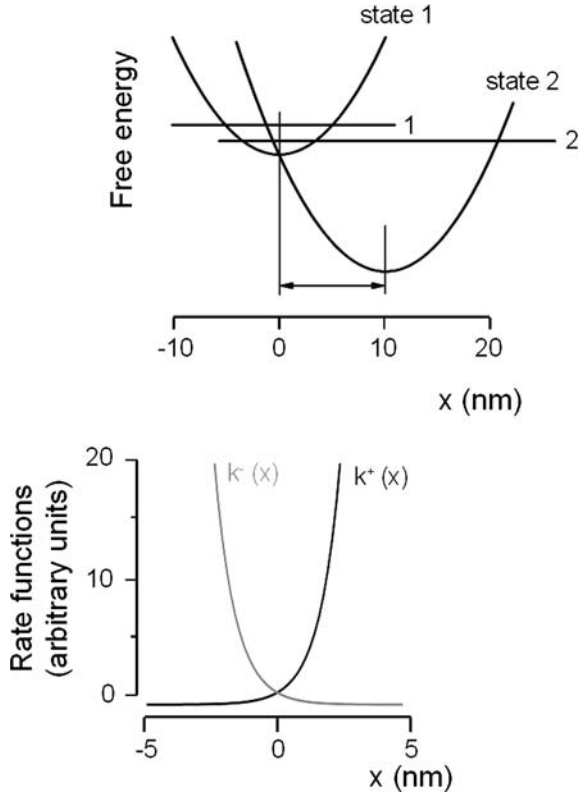

Fig. 6. Free energy functions and rate functions used in the modeling. Top panel, free energy functions of initially attached state (state 1) and corresponding detached state (1). Minimum of free energy function of state 1 is just slightly below free energy level of corresponding detached state; i.e., state 1 is only weakly attached. Free energy function of second attached state (state 2) is shifted relative to free energy function of state 1. Horizontal shift equals assumed stroke size (10 nm), vertical shift selected such that free energy function of state 2 crosses through minimum of free energy function of state 1 (Hill, 1974). Shape of free energy functions of state 1 and state 2 results from assumption of linear elasticity of myosin head of 1 pN/nm. Bottom panel, rate functions to define strain dependence of forward and reverse rate constants for transition from state 1 to state 2. Equal partitioning of strain dependence between the forward and reverse rate constant assumed. Shape of rate functions then results from difference of free energy ($\Delta G_{1,2}$) vs. head distortion (x) specified by the relative position of the free energy functions of state 1 and state 2.

distortion of the myosin head in the initially attached state ($F_{\text{head}}(x) = k_{\text{head}}x$). In the third step equilibrium binding in the first attached state was calculated for different dumbell positions (ξ), considering head distortion (x) and its effects on the equilibrium-binding constant for the weak attachment. Strain dependence of the equilibrium-binding constant is defined by the free energy difference between state 1 and the related detached state (labeled '1' in Figrue 6). The fourth step was to calculate the probability to execute the power stroke after initial attachment at the dumbell position ξ, considering the effect of head distortion (x) on the rate constants associated with the power stroke, i.e., the transition from state 1 to state 2. While $K_{1,2}(x)$ and thus $k_{1,2}{}^{+}(x)/k_{1,2}{}^{-}(x)$ were specified by the free energy functions we initially used equal partitioning of strain-dependence for the two rate constants. I.e., $k_{1,2}{}^{+}(x) = \exp(-0.5\Delta G_{1,2}(x)/k_{\text{B}}T)$ and $k_{1,2}{}^{-}(x) = \exp(0.5\ \Delta G_{1,2}(x)/k_{\text{B}}T)$. In the fifth step the resulting dumbell position after execution of the power stroke was calculated, again considering that the actual dumbell position results from the balance of trapping forces and elastic forces from distortion of the attached myosin head by the trapping forces. In the last step, the expected probability to observe an event (with power stroke) at a certain dumbell position was plotted as a function of dumbell position (ξ). Finally, a Gaussian function was fit to the resulting 'position histogram', equivalent to the procedure introduced by Molloy *et al.* (1995). As a result, the shift of the position histogram relative to the free dumbell position was obtained as a measure of the 'observed' power stroke.

The Gaussian functions shown in Figure 5, including the black Gaussian function, actually represent histograms calculated by this modeling for a head stiffness of 1 pN/nm, a trap stiffness of 0.01 pN/nm, and an assumed stroke size of 10 nm. The red function is the position histogram of the free dumbell, the green function is the position histogram with the assumption that the traps do not exert any forces onto the tethered dumbell, i.e., on the attached myosin head, and the black trace was obtained for the more realistic situation in which the trapping forces due to displacement of the dumbell (ξ) away from its equilibrium position are equal in magnitude but of opposite direction to the elastic forces exerted by the attached myosin head when distorted by the trapping forces. Changing the free energy difference between the unattached myosin head and the initially attached state at its minimum free energy, i.e., varying the binding affinity of the initially attached state had essentially no effect on the position of the calculated histogram (black line in Figure 5d), only the total number of expected events was affected. The calculated histogram (black line in Figure 5d) has a Gaussian shape of almost the same width as the thermal fluctuation of the free dumbell. It is, however, only shifted by about 5 nm to the right (in the direction of the power stroke). Therefore, the observed shift of the histogram is only about 50% of the stroke size put into the model (horizontal shift of the second attached state relative to the initially attached state) which was set to 10 nm.

In conclusion, the 'apparent' stroke size (displacement of the position histogram from its equilibrium position) is smaller than the displacement generated by an attached myosin head during its power stroke (equivalent to the horizontal shift of the free energy functions of the two attached states). The difference is caused by distortion of the attached myosin head by trapping forces that tend to pull the dumbell toward its equilibrium position. Distortions of the attached myosin head affect the probability to execute the power stroke (transition from state 1 to state 2) in such a way that the position histogram is much less shifted away from the zero position than expected without distortion of the attached myosin head (cf. Figures 4 and 5d).

Effects of trap stiffness on "observed stroke size"

To explore the parameters that determine the difference between observed stroke size and the stroke size put into the model, we first examined effects of the magnitude of the trap stiffness. Very low trap stiffness was previously thought to be sufficient to exclude detectable effects of trapping forces on the observed stroke size (shift of position histograms). To test this assumption we examined the shift in position histograms ('apparent' stroke size) for a large range of trap stiffnesses, starting from 1 pN/nm, i.e., equal to the stiffness of the myosin head, down to 0.0001 pN/nm. This includes trap stiffnesses in the range around 0.01 pN/nm that is usually used in single molecule trapping experiments. All other parameters of the model were kept unchanged.

As shown in Figure 7, the observed stroke size stays very close to 5 nm for all trap stiffnesses below 0.1 pN/nm compared to the 'true' stroke size of 10 nm that was one of the model assumptions. At trap stiffness above 0.1 pN/nm the observed stroke size becomes less than 5 nm. Note that although trap stiffness is reduced, at trap stiffnesses below 0.1 pN/nm there is essentially no change in observed stroke size. Apparently distortion of the attached head is still relevant even at these low trap stiffnesses. This presumably reflects the fact that as trap stiffness (k_{trap}) is reduced, the amplitude of thermal fluctuations of the dumbell increases. Note that the mean squared displacement of the dumbell during thermal fluctuations ($\langle\xi^2\rangle$) is related to trap stiffness (k_{trap}) by $k_{trap}\langle\xi^2\rangle = k_B T$, where k_B is Boltzmann constant and T is absolute temperature. At any rate, the modeling shows that reduction in trap stiffness apparently does not reduce distortions of the attached myosin head to an irrelevant level such that the 'apparent' stroke size (shift of position histogram) approaches the 'true' stroke size.

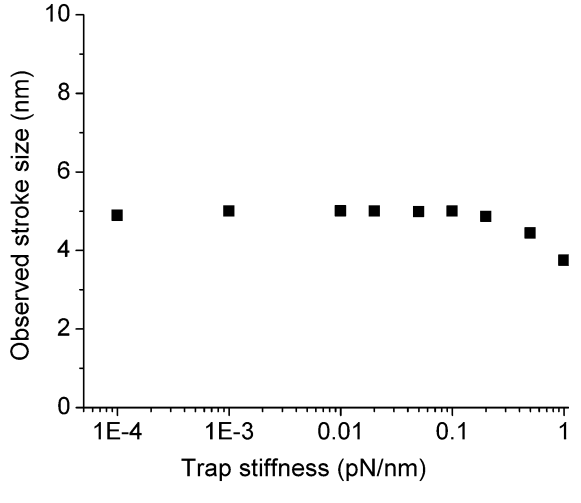

Fig. 7. Observed stroke size expected for different trap stiffnesses. Calculated shift of position histogram is plotted against assumed trap stiffness. Stiffness of myosin head assumed to be 1 pN/nm, displacement generated during work stroke, i.e., horizontal shift between free energy functions of state 1 and state 2, was set to 10 nm. Note that trap stiffness in single molecule experiments is usually around 0.01 pN/nm.

In conclusion, reduction in trap stiffness does not prevent discrepancies between the displacement generated during the power stroke (equal to the horizontal shift of the free energy functions of the two attached states) and the 'observed' stroke size derived from the shift of the position histogram.

Effect of lever arm length on observed stroke size

Next we examined whether the difference between 'true' stroke size and 'observed' stroke size changes with lever arm length since a change in this difference would profoundly affect the conclusions drawn from our single molecule studies with myosin constructs of different lever arm length. For this part of the modeling, we made the following assumptions: (1) the crossover between the free energy functions of state 1 and state 2 was kept at the free energy minimum of state 1; (2) the assumed stroke size, i.e., the horizontal shift between the free energy profiles of the two attached states, is proportional to lever arm length; (3) stiffness of the myosin head was assumed to be inversely proportional to the square of the lever arm length, equivalent to a system of a pivotal spring with the remaining lever arm acting as a rigid body (cf. Köhler *et al.*, 2002); in a second set, stiffness of the myosin head was assumed to be inversely proportional to the cube of the lever arm length, equivalent to elastic bending along the full length of the lever arm (cf. Howard and Spudich, 1996). (4) The strain dependence of the transition from state 1 to state 2 was equally partitioned between forward and reverse rate constant.

For all lever arm lengths, and for both types of compliance within the lever arm, the observed stroke size from the histogram technique is predicted to be very close to half of the horizontal shift of the free energy functions of the two attached states, i.e., half of the 'true' power stroke. These results imply that the actual displacement generated during the power stroke for the different *Dictyostelium discoideum* myosin II-constructs is twice the value of the 'apparent' stroke observed with the histogram technique (Ruff *et al.*, 2001b). The expected filament sliding during the power stroke was replotted against lever arm length (Figure 8). Since for all lever arm lengths, and independent on the distribution of elastic bending within the lever arm, the observed stroke size was off by the same factor, the point of intersection of the line fitted by least squares minimization procedure remained near −2 nm (Figure 8).

In conclusion, in spite of the apparent difference between 'observed' and 'true' stroke sizes, our previous conclusions that the stroke size appears to be proportional to the lever arm length and that the pivot point of lever arm rotation is about 2 nm inside the catalytic domain (Ruff *et al.*, 2001b) remain valid.

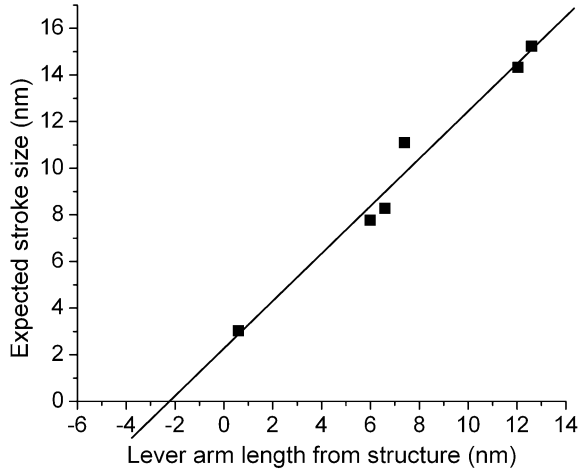

Fig. 8. Expected stroke size ('true' stroke size), i.e., distance of filament sliding generated during the power stroke vs. length of light chain binding domain or artificial lever arm element composed of α-actinin repeats. Expected stroke size was calculated from 'observed' stroke size (= horizontal shift of position histogram) and the extent by which stroke size is underestimated by histogram technique (50% for all lever arm lengths).

Relation between lever arm length and observed stroke size: Effect of strain dependence in the forward reaction of power stroke

Comparison of the plot of 'apparent' stroke size vs. lever arm length for *Dictyostelium discoideum* myosin II constructs with plots for class-I myosin (Myo 1d; cf. Figure 2; Kohler *et al.*, 2003) showed that at similar lever arm lengths class-I myosin can generate an 'apparent' stroke of almost three-times the size seen for the class-II skeletal muscle myosin. Although the rotation of the converter domain of class-I myosin was found to be about 30° larger than for the *Dictyostelium discoideum* class-II myosins, the extra 30° of lever arm rotation alone cannot account for the almost three-times larger stroke size (cf. Figure 3b). We therefore examined whether we can identify at least some parameters that may affect the extent of the discrepancy between 'observed' stroke size, derived from the histogram approach, and 'true' stroke size which equals the actual filament sliding during the power stroke, i.e., the horizontal shift between the free energy functions of the two attached states in our model calculations.

One factor we could find to affect the extent of difference between 'observed' and 'true' stroke size is the partitioning of the strain dependence between forward and reverse rate constants for the transition from the initially attached state (state 1) to the strongly attached state (state 2). With all other assumptions unchanged, we only varied the fraction of strain dependence in the forward rate constant, keeping the ratio of $k_{1,2}^{+}(x)/k_{1,2}^{-}(x)$ constant and equal to $K_{1,2}(x) = \exp(-\Delta G_{1,2}(x)/k_{\mathrm{B}}T)$, where $\Delta G_{1,2}(x)$ is free energy difference between state 1 and state 2 as specified by the free energy functions of state 1 and state2 (cf. Figure 6a). Figure 9d shows plots of 'observed' stroke size vs. lever arm length for the usual equal partitioning (0.5 = 50% in rate function for forward, 50% in rate function for reverse reaction; cf. Figure 9b), reduced strain dependence in the forward reaction (0.3 = 30% in rate function for forward reaction, 70% in rate function for reverse reaction; cf. Figure 9a), and increased strain dependence in forward reaction (0.7 = 70% in rate function for forward reaction, 30% in reverse reaction; cf. Figure 9c). The dashed line in Figure 9d is the expected plot for the 'true' stroke size vs. lever arm length. Note that different extent of strain dependence in the forward reaction affects the discrepancy between 'observed' and 'true' stroke size. As a consequence, even for constructs that show no difference in 'true' stroke size (dashed line in Figure 9d), somewhat different strain dependence of the forward reaction of the power stroke can generate a difference in the plots of 'observed' stroke size vs. lever arm length. Thus, it is well possible that part of the large difference in the 'observed' stroke size between class-I and class-II myosins may be due to e.g. somewhat smaller strain dependence in the forward reaction of the power stroke (state 1 to state 2) for class I myosins. Thus, different strain dependence in the forward reaction can in principle account for the discrepancy between structural data (30° larger rotation of the converter) and the almost 3−fold larger 'apparent' stroke size.

Similarly, the different slopes when 'apparent' stroke size is plotted vs. lever arm length for smooth muscle myosin II or myosin V may again at least in part be due to differences in the strain dependence (strain sensitivity) of the forward reaction in the power stroke rather than be the result of different extent of converter domain rotation.

In conclusion, the slope of plots of apparent stroke size vs. lever arm length is not only sensitive to the extent of converter domain/lever arm rotation but is also sensitive to the extent of strain dependence in the forward/reverse reaction of the power stroke. Thus, different stroke size at the same lever arm length is not necessarily a direct indication of different extent of converter domain/lever arm rotation but may also result from different strain dependence of the forward and reverse reaction of the power stroke.

Limitations of modeling experimental data

In our modeling we assumed that any event that has proceeded into the strongly bound state will be detected. This assumption, however, has some clear limitations. For instance, assuming smaller strain dependence in the forward reaction of the power stroke results in increased strain dependence of the reverse reaction with much faster reverse reaction for strain opposing the power stroke (negative x). This would result in (i) an increasing number of events being terminated by reversal of the power stroke, and (ii) by a reduction in the life-time of events in state 2. As a consequence, limited time resolution for detection of

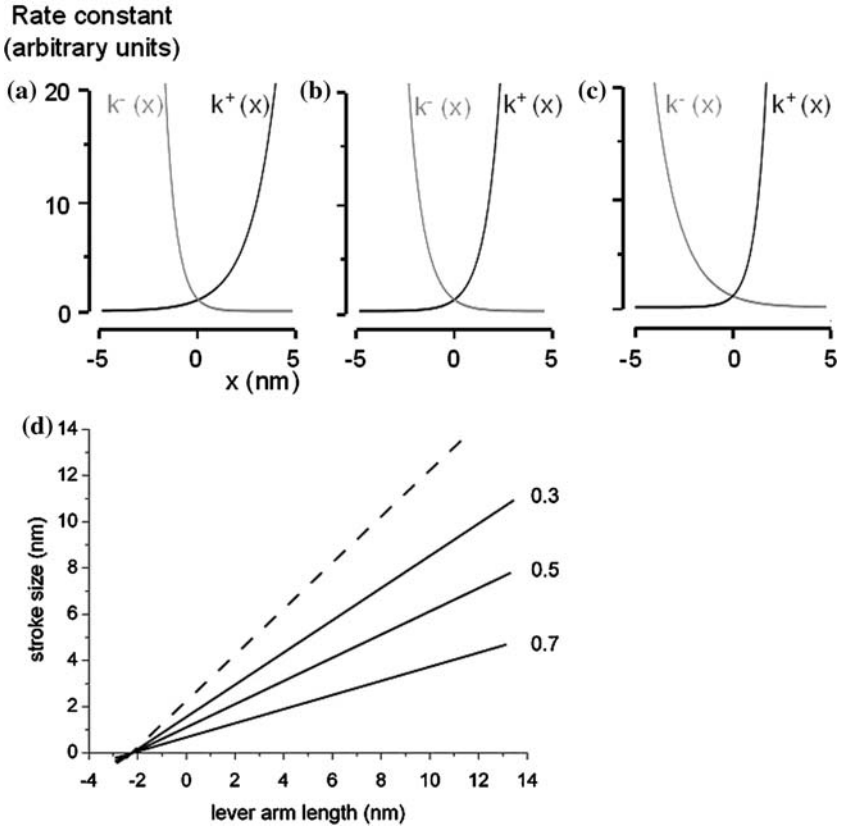

Fig. 9. Effect of partitioning of strain dependence between forward and reverse rate of power stroke on apparent stroke size. (a)–(c) show rate functions used in the modeling; $k^{+}(x) = \exp(-n\Delta G_{1,2}(x)/k_{B}T$ and $k^{-}(x) = \exp((1-n)\Delta G_{1,2}(x)/k_{B}T)$ with n = fraction of partitioning; $n = 0.3$, 0.5, and 0.7 for (a), (b), and (c), respectively; $\Delta G_{1,2}(x)$ = difference in free energy between state 1 and state 2 at different strain of myosin motor domain. k_{B} = Boltzmann constant. (d) Plots of 'observed' stroke size vs. lever arm length for different partitioning of strain dependence between forward and reverse rate of power stroke. Number next to each trace is fraction (n) of strain dependence in rate function for forward reaction. Dashed line is 'true' stroke size vs. lever arm length. 'True' stroke size equals the horizontal distance between the minima of free energy functions of state 1 and state 2; this distance is assumed to be proportional to lever arm length. Pivot point assumed to be −2 nm inside the motor domain; lever arm length = length of light chain binding domain or of artificial replacement (e.g., construct of α-actinin repeats). Note that at a given lever arm length the 'apparent' stroke size = shift of position histogram varies with the fraction of strain-dependence in forward rate of power stroke.

binding events would lead to an increasing number of missed, short-lived events. The reduction in life-time and thus the fraction of short lived events, however, are not equal for all strains of the attached myosin head. Instead, these effects would preferentially be found where the free energy difference between state 1 and 2 is small or even reversed (negative x). This is on the side of the position histogram where the trapping forces generate strain against the direction of the power stroke, i.e., on the right hand side of the position histogram (cf. Figure 4, solid arrows labeled ξ and x). Thus, increased strain dependence in the reverse reaction of the power stroke will decrease the number of events detected on the right hand part of the position histogram. Events on the left hand side of the position histogram, however, would have longer life-time and thus be more effectively detected. Overall, with increasing strain dependence in the reverse reaction of the power stroke an increasing deficit in event detection will occur. This will result in increasing changes in the observed position histograms in the same way as illustrated in Figure 5c and d, and thus will more and more reduce the observed stroke size. The extent to which the observed shift of the position histogram will actually be reduced, and thus the extent to which the stroke size will be underestimated, however, will be dominated by the actual time resolution of the equipment, i.e., by the minimum life time of events that is necessary for their successful detection. Thus, even if some myosin molecules had all strain dependence in the reverse reaction of the power stroke we still would expect to observe a shift in the position histogram that is smaller than the true power stroke.

Implications

Molloy *et al.* (1995) had introduced the concept that the shift of position histograms of myosin binding events in double trap experiments represents the size of the power stroke, or at least of its first step for molecules with a distinct second (or even further) step. This concept was based on the assumption that binding of the myosin head to actin can occur with equal probability at any site along the actin filament, i.e., the probability of attachment to any site on actin is only

determined by the position of the dumbell during free thermal fluctuation. The second essential assumption for this concept is that the power stroke will be executed with identical probability at any position of initial attachment. Here we showed that even for the most simple model describing the interaction of a myosin motor domain with an actin filament this second condition is very crucial and presumably never met. Even in the case of strain independent forward reaction into the power stroke the change in life-time of events, due to increased strain dependence of the reverse reaction, will again 'truncate' the observed shift in the position histogram due to inability to detect short lived events with the current limitations of time resolution for event detection.

Such truncation effects are expected to be relevant not only for the histogram-approach of Molloy *et al.* (1995), but any approach in which overall effects of many events are analyzed will be affected if the individual events, due to thermal fluctuations of one of the interaction partners (actin filament or myosin motor domain), take place at different locations along the actin filament, such that the attached motor domain is distorted to different extent by the forces driving e.g. the bead/dumbell back to its equilibrium position. Thus, the event averaging approach (Veigel *et al.*, 1999) or the mean-variance analysis (Guilford *et al.*, 1997) are expected to yield similar underestimates of the actual stroke size as the histogram-approch. In addition, the problem is not limited to the dumbell arrangement. Instead, single bead trapping or equivalent approaches are expected to be affected as well.

We demonstrated that due to strain-induced differences in the probability to execute the power stroke at different dumbell positions (i) the observed power stroke is very likely significantly underestimated. (ii) The discrepancy between shift of the position histogram ('observed' stroke size) and the 'true' stroke size does not disappear when trap stiffness is reduced. (iii) We also demonstrated that at the same lever arm length the stroke size observed with the histogram approach varies with the strain sensitivity for forward/reverse rate of the power stroke even if the 'true' stroke size is constant. Thus, differences in the 'apparent' stroke size among different myosins that are not accounted for by differences in converter domain/lever arm rotation can quite easily result from somewhat different strain sensitivity of the forward/reverse rate of the power stroke.

As a consequence, the differences between stroke sizes expected from protein crystallography and observed stroke sizes in single molecule experiments to a large extent are very likely caused by this underestimate of the actual stroke size in the position histogram or related approaches. We therefore have to devise procedures that allow to directly determine the actual stroke size or that allow to reliably derive the true stroke size from the stroke size observed with the position histogram technique or by related approaches.

Acknowledgement

This work was supported by the DFG-Priority Program 'Molecular Motors' (SPP 1068) grants Br 849/21–1,2,3.

References

Anson M, Geeves MA, Kurzawa SE and Manstein DJ (1996) Myosin motors with artificial lever arms. *Embo J* **15:** 6069–6074.

Brenner B (1988) An experimental approach to determine cross-bridge turnover kinetics during isometric and isotonic steady state contraction using skinned skeletal muscle fibres of the rabbit. *Pflügers Arch* **411:** R186.

Brenner B (1990) In: Squire J (ed) *Molecular Mechanism of Muscular Contraction*. (pp. 77–149). Macmillan, London.

Burton K (1992) Myosin step size: estimates from motility assays and shortening muscle. *J Muscle Res Cell Motil* **13:** 90–607.

Carragher BO, Cheng N, Wang ZY, Korn ED, Reilein A, Belnap DM, Hammer JA III and Steven AC (1998) Structural invariance of constitutively active and inactive mutants of acanthamoeba myosin IC bound to F-actin in the rigor and ADP-bound states. *Proc Natl Acad Sci USA* **95:** 15206–15211.

Chen YD and Brenner B (1993) On the regeneration of the actin–myosin power stroke in contracting muscle. *Proc Natl Acad Sci USA* **90:** 5148–5152.

Cooke R (1986) The mechanism of muscle contraction. *CRC Crit Rev Biochem* **21:** 53–118.

Corrie JE, Brandmeier BD, Ferguson RE, Trentham DR, Kendrick-Jones J, Hopkins SC, Van Der Heide UA, Goldman YE, Sabido-David C, Dale RE, Criddle S and Irving M (1999) Dynamic measurement of myosin light-chain-domain tilt and twist in muscle contraction. *Nature* **400:** 425–430.

Finer JT, Simmons RM and Spudich JA (1994) Single myosin molecule mechanics: piconewton forces and nanometre steps. *Nature* **368:** 113–119.

Ford LE, Huxley AF and Simmons RM (1977) Tension responses to sudden length change in stimulated frog muscle fibres near slack length. *J Physiol (Lond)* **269:** 441–515.

Geeves MA and Holmes KC (1999) Structural mechanism of muscle contraction. *Annu Rev Biochem* **68:** 687–728.

Guilford WH, Dupuis DE, Kennedy G, Wu J, Patlak JB and Warshaw DM (1997) Smooth muscle and skeletal muscle myosins produce similar unitary forces and displacements in the laser trap. *Biophys J* **72:** 1006–1021.

Harada Y, Sakurada K, Aoki T, Thomas DD and Yanagida T (1990) Mechanochemical coupling in actomyosin energy transduction studied by in vitro movement assay. *J Mol Biol* **216:** 49–68.

Higuchi H and Goldman YE (1991) Sliding distance between actin and myosin filaments per ATP molecule hydrolysed in skinned muscle fibres. *Nature* **352:** 352–354.

Hill TL (1974) Theoretical formalism for the sliding filament model of contraction of striated muscle. Part I. *Prog Biophys Mol Biol* **28:** 267–340.

Homsher E, Irving M and Wallner A (1981) High-energy phosphate metabolism and energy liberation associated with rapid shortening in frog skeletal muscle. *J Physiol (Lond)* **321:** 423–436.

Howard J and Spudich JA (1996) Is the lever arm of myosin a molecular elastic element?. *Proc Natl Acad Sci USA* **93:** 4462–4464.

Huxley AF (1957) Muscle structure and theories of contraction. *Prog Biophys Biophys Chem* **7:** 255–318.

Huxley AF and Simmons RM (1971) Proposed mechanism of force generation in striated muscle. *Nature* **233:** 533–538.

Huxley AF and Simmons RM (1973) Mechanical transients and the origin of muscular force. *Cold Spring Harb Symp Quant Biol* **37:** 669–680.

Huxley HE, Stewart A, Sosa H and Irving T (1994) X-ray diffraction measurements of the extensibility of actin and myosin filaments in contracting muscle. *Biophys J* **67:** 2411–2421.

Jontes JD and Milligan RA (1997) Brush border myosin-I structure and ADP-dependent conformational changes revealed by cryoelectron microscopy and image analysis. *J Cell Biol* **139:** 683–693.

Jontes JD, Ostap EM, Pollard TD and Milligan RA (1998) Three-dimensional structure of Acanthamoeba castellanii myosin-IB (MIB) determined by cryoelectron microscopy of decorated actin filaments. *J Cell Biol* **141:** 155–162.

Jontes JD, Wilson-Kubalek EM and Milligan RA (1995) A 32 degree tail swing in brush border myosin I on ADP release. *Nature* **378:** 751–753.

Kliche W, Fujita-Becker S, Kollmar M, Manstein DJ and Kull FJ (2001) Structure of a genetically engineered molecular motor. *Embo J* **20:** 40–46.

Kohler D, Ruff C, Meyhofer E and Bahler M (2003) Different degrees of lever arm rotation control myosin step size. *J Cell Biol* **161:** 237–241.

Köhler J, Winkler G, Schulte I, Scholz T, Mckenna W, Brenner B and Kraft T (2002) Mutation of the myosin converter domain alters cross-bridge elasticity. *Proc Natl Acad Sci USA* **99:** 3557–3562.

Kollmar M, Durrwang U, Kliche W, Manstein DJ and Kull FJ (2002) Crystal structure of the motor domain of a class-I myosin. *Embo J* **21:** 2517–2525.

Molloy JE, Burns JE, Kendrick-Jones J, Tregear RT and White DC (1995) Movement and force produced by a single myosin head. *Nature* **378:** 209–212.

Pate E, White H and Cooke R (1993) Determination of the myosin step size from mechanical and kinetic data. *Proc Natl Acad Sci USA* **90:** 2451–2455.

Piazzesi G, Lucii L and Lombardi V (2002) The size and the speed of the working stroke of muscle myosin and its dependence on the force. *J Physiol* **545:** 145–151.

Purcell TJ, Morris C, Spudich JA and Sweeney HL (2002) Role of the lever arm in the processive stepping of myosin V. *Proc Natl Acad Sci USA* **99:** 14159–14164.

Rayment I, Holden HM, Whittaker M, Yohn CB, Lorenz M, Holmes KC and Milligan RA (1993a) Structure of the actin–myosin complex and its implications for muscle contraction. *Science* **261:** 58–65.

Rayment I, Rypniewski WR, Schmidt-Base K, Smith R, Tomchick DR, Benning MM, Winkelmann DA, Wesenberg G and Holden HM (1993b) Three-dimensional structure of myosin subfragment−1: a molecular motor. *Science* **261:** 50–58.

Reconditi M, Linari M, Lucii L, Stewart A, Sun YB, Boesecke P, Narayanan T, Fischetti RF, Irving T, Piazzesi G, Irving M and Lombardi V (2004) The myosin motor in muscle generates a smaller and slower working stroke at higher load. *Nature* **428:** 578–581.

Ruff C, Brenner B and And Meyhöfer E (2001a) The step size of myosin II is orientationally independent. *Biophys J* **80:** 78a.

Ruff C, Furch M, Brenner B, Manstein DJ and Meyhofer E (2001b) Single-molecule tracking of myosins with genetically engineered amplifier domains. *Nat Struct Biol* **8:** 226–229.

Schroder RR, Manstein DJ, Jahn W, Holden H, Rayment I, Holmes KC and Spudich JA (1993) Three-dimensional atomic model of F-actin decorated with Dictyostelium myosin S1. *Nature* **364:** 171–174.

Sleep J, Lewalle A and Smith DA (2005) Displacements in the optical trap underestimate the myosin working stroke by a factor of two. *Biophys J* **88:** 3110(Abstr.).

Smith CA and Rayment I (1996) X-ray structure of the magnesium(II).ADP.vanadate complex of the Dictyostelium discoideum myosin motor domain to 1.9 A resolution. *Biochemistry* **35:** 5404–5417.

Steffen W, Smith D, Simmons R and Sleep J (2001) Mapping the actin filament with myosin. *Proc Natl Acad Sci USA* **98:** 14949–14954 Epub 12001 Dec 14944.

Tanaka H, Homma K, Iwane AH, Katayama E, Ikebe R, Saito J, Yanagida T and Ikebe M (2002) The motor domain determines the large step of myosin-V. *Nature* **415:** 192–195.

Tanaka H, Ishijima A, Honda M, Saito K and Yanagida T (1998) Orientation dependence of displacements by a single one-headed myosin relative to the actin filament. *Biophys J* **75:** 1886–1894.

Uyeda TQ, Abramson PD and Spudich JA (1996) The neck region of the myosin motor domain acts as a lever arm to generate movement. *Proc Natl Acad Sci USA* **93:** 4459–4464.

Veigel C, Coluccio LM, Jontes JD, Sparrow JC, Milligan RA and Molloy JE (1999) The motor protein myosin-I produces its working stroke in two steps. *Nature* **398:** 530–533.

Wakabayashi K, Sugimoto Y, Tanaka H, Ueno Y, Takezawa Y, Amemiya Y (1994) X-ray diffraction evidence for the extensibility of actin and myosin filaments during muscle contraction [published erratum appears in *Biophys J* 1995 Mar; **68**(3)**:** 1196–1197]. *Biophys J* **67:** 2422–2435.

Warshaw DM, Guilford WH, Freyzon Y, Krementsova E, Palmiter KA, Tyska MJ, Baker JE and Trybus KM (2000) The light chain binding domain of expressed smooth muscle heavy meromyosin acts as a mechanical lever. *J Biol Chem* **275:** 37167–37172.

Yanagida T, Arata T and Oosawa F (1985) Sliding distance of actin filament induced by a myosin crossbridge during one ATP hydrolysis cycle. *Nature* **316:** 366–369.